Supplementary Information (SI) for Journal of Materials Chemistry C.

High-performance WS_2/ZnO QDs heterojunction photodetector with charge and energy transfer

Yanjie Zheng,[a] Zhe Xu,[b] Kaixi Shi,*[a] Jinhua Li,*[a] Xuan Fang,[c] Zhenfeng Jiang,[a] Xueying Chu[a]

a. Nanophotonics and Biophotonics Key Laboratory of Jilin Province, School of Physics, Changchun University of Science and Technology, Changchun, Jilin 130022, People's Republic of China

b. Changchun High-tech Industrial Development Zone, Shangde Academy of Jilin University, Changchun, Jilin 130000, People's Republic of China

c. State Key Laboratory of High Power Semiconductor Laser, School of Science, Changchun University of Science and Technology, Changchun, Jilin 130022, People's Republic of China

E-mail: shikaixi@cust.edu.cn, lijh@cust.edu.cn

Supporting Information

1. Preparation process and optical characterization of ZnO QDs.

Figure S1a shows the synthesis steps of zinc oxide quantum dots with oxygen interstitials. Figures S1b and c show the absorption and luminescence spectra of ZnO QDs at different concentrations, respectively. At a concentration of 18 mmol/L, the luminescence intensity of ZnO QDs is the strongest. This is attributed to the appropriate concentration of QDs suppressing their aggregation. Strong luminescence will generate a larger spectral overlap with the absorption of WS_2, which facilitates dipole-dipole interactions and creates conditions for non-radiative energy transfer. Next, the bandgap of ZnO QDs was calculated by the following equation:

$$(\alpha \cdot hv)^2 = B \cdot (hv - E_g)$$

where α is the absorption coefficient, h is the Planck's constant, v is the frequency of the incident light, and B is a constant. As shown in Figure S1d, the bandgap of ZnO QDs was about 3.34 eV.

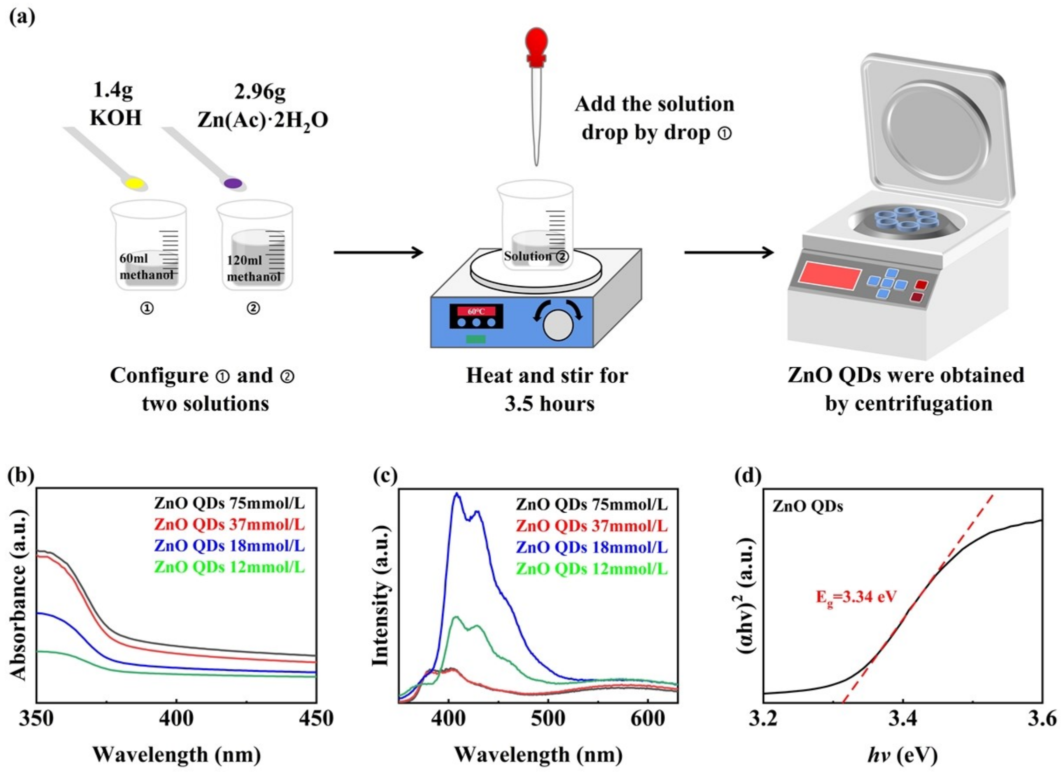

Figure S1. (a) Synthesis steps of ZnO QDs using the sol-gel method. Absorption spectra (b) and luminescence spectra (c) of ZnO QDs at different concentrations. (d) Bandgap of 18 mmol/L ZnO QDs.

2.The UV photoresponse of the WS_2 and WS_2/ZnO QDs devices under 325 nm laser irradiation.

To demonstrate the broad spectral response of WS_2/ZnO heterojunction photodetector, the UV photoresponse of the device was tested under 325 nm laser irradiation. As shown in the Figure S2a-b, the WS_2 device and the WS_2/ZnO device exhibit UV photoresponse. As shown in the Figure S2c-d, the WS_2/ZnO device exhibits enhanced UV photoresponse under 325 nm laser irradiation with different optical power densities. As a result, a UV-visible photodetector based WS_2/ZnO heterojunction was achieved.

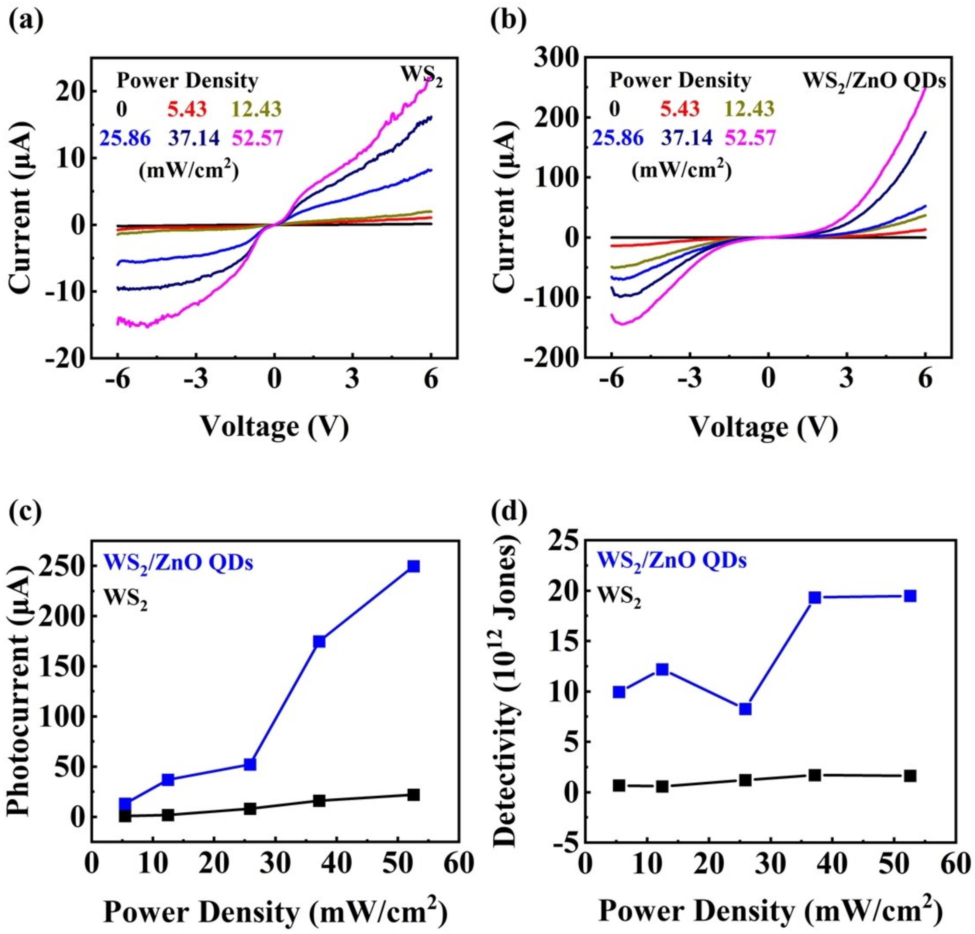

Figure S2. The I-V curves of WS_2 (a) and WS_2/ZnO QDs (b) photodetectors under 325 nm laser irradiation with different optical power densities. The dependence of photocurrent (c) and detectivity (d) for WS_2 and WS_2/ZnO QDs photodetectors under 325 nm laser irradiation with different optical power densities.

3. The energy band diagram of the WS_2/Al_2O_3/ZnO QDs device.

Figure S3 shows the energy band diagram of the WS_2/Al_2O_3/ZnO QDs device. To confirm the non-radiative energy transfer in the WS_2/ZnO QDs heterojunction, we designed the WS_2/Al_2O_3/ZnO QDs heterojunction. The wide bandgap Al_2O_3 acts as a barrier to inhibit the charge transfer between WS_2 and ZnO QDs. The bandgap of Al_2O_3 is much wider than that of monolayer WS_2 and ZnO QDs, which prevents charge transfer. As a result, the WS_2/Al_2O_3/ZnO QDs device is only driven by non-radiative energy transfer.

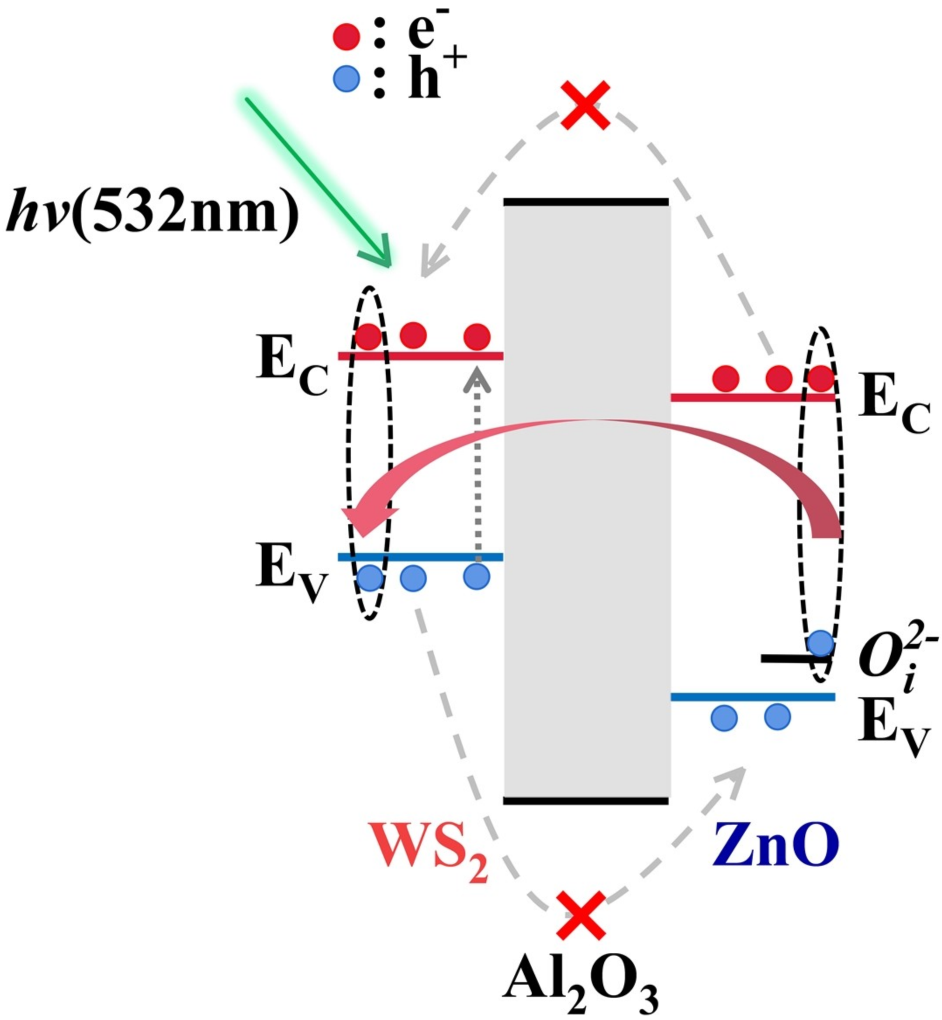

Figure S3. Energy band diagram of the WS_2/Al_2O_3/ZnO QDs device.